Ultrasonics 62 (2015) 136–146

Contents lists available at ScienceDirect

Ultrasonics

journal homepage: www.elsevier.com/locate/ultras

Screen-printed ultrasonic 2-D matrix array transducers for microparticle manipulation

Yongqiang Qiu [a,*], Han Wang [a], Sylvia Gebhardt [b], Aleksandrs Bolhovitins [a], Christine E.M. Démoré [a], Andreas Schönecker [b], Sandy Cochran [a]

[a] Institute for Medical Science and Technology, University of Dundee, Dundee, United Kingdom
[b] Fraunhofer Institute for Ceramic Technologies and Systems, Dresden, Germany

ARTICLE INFO

Article history:
Received 25 March 2015
Received in revised form 17 May 2015
Accepted 17 May 2015
Available online 23 May 2015

Keywords:
Thick film
Screen-printing
2-D matrix array
Particle manipulation

ABSTRACT

This paper reports the development of a two-dimensional thick film lead zirconate titanate (PZT) ultrasonic transducer array, operating at frequency approximately 7.5 MHz, to demonstrate the potential of this fabrication technique for microparticle manipulation. All layers of the array are screen-printed then sintered on an alumina substrate without any subsequent patterning processes. The thickness of the thick film PZT is 139 ± 2 μm, the element pitch of the array is 2.3 mm, and the dimension of each individual PZT element is 2 × 2 mm^2 with top electrode 1.7 × 1.7 mm^2. The measured relative dielectric constant of the PZT is 2250 ± 100 and the dielectric loss is 0.09 ± 0.005 at 10 kHz. Finite element analysis was used to predict the behaviour of the array and to optimise its configuration. Electrical impedance spectroscopy and laser vibrometry were used to characterise the array experimentally. The measured surface motion of a single element is on the order of tens of nanometres with a 10 V_{peak} continuous sinusoidal excitation. Particle manipulation experiments have been demonstrated with the array by manipulating Ø10 μm polystyrene microspheres in degassed water. The simplified array fabrication process and the bulk production capability of screen-printing suggest potential for the commercialisation of multilayer planar resonant devices for ultrasonic particle manipulation.

1. Introduction

Contactless microparticle manipulation technologies, such as optical tweezing [1], dielectrophoresis [2], and ultrasonic manipulation [3] have been in rapid development to demonstrate how increasing demand may be met for precise manipulation of bio-particles, cells and molecules in cell biology and analytical chemistry. In ultrasonic manipulation (USM) devices, the objects can be manipulated by either gradient forces caused by ultrasonic standing waves (USWs) [3–8] or momentum transferred from propagating ultrasound beams [9–12]. Because of the use of ultrasound, USM has shown good ability to maintain cell viability through controlled acoustic intensity, avoiding the likelihood of cavitation [13–16]. Given other advantages of USM devices, such as the ability to handle a large number of cells, a range of biological and medical applications have been demonstrated in microfluidic systems and bioassays [7,17], e.g. cell sorting [18–20], cell patterning [5,21,22], tissue engineering [23,24] and studies of cell motility and structure [25,26]. USM also has the ability to coexist with other manipulation technologies, leading to a broader range of microfluidic applications with combined advantages from different technologies, such as maintaining high throughput with improved precision of individual particle manipulation [27–31].

To increase the dexterity of an USM device, one straightforward approach is to use multiple ultrasound sources. Manneberg et al. used four wedge transducers to realise spatially confined particle separation [32]. Counter-propagating ultrasound waves generated from four or more transducers were used in patterning particles and cells [33–36]. More recently, independent trapping and manipulation of multiple individual microparticles were demonstrated with an electronically controlled 64-element circular transducer array [37]. The use of a one-dimensional (1-D) ultrasound array to manipulate particle agglomerates perpendicular to the direction of wave propagation was also studied [38–40]. Although implementation of two-dimensional (2-D) arrays could increase dexterity [10,12], this is still relatively rare in the literature, partly because of the challenges in fabrication, electrical interconnection and system integration of reliable, miniature 2-D arrays based on traditional machining and packaging methods. These challenges

* Corresponding author.
E-mail address: yqiu@ieee.org (Y. Qiu).

http://dx.doi.org/10.1016/j.ultras.2015.05.010
0041-624X/

also negatively affect the progress towards mass production and commercialisation of such USM devices.

Thick film technologies have significant advantages in simplifying fabrication and allowing miniaturisation for functional integration. Piezoelectric thick films have already been explored for high frequency ultrasonic single element transducers and linear arrays for medical imaging [41–43]. Depending on the desired thickness and shape of the PZT film, different thick film techniques can be used, such as modified sol–gel [44], hydrothermal deposition [45], aerosol deposition [46], electrophoretic deposition [47], ink-jet printing [48], pad-printing [49] and screen-printing [50]. Among these methods, screen-printing allows relatively simple fabrication of patterned films with typical thicknesses between 10 and 150 μm with excellent reproducibility. Furthermore, the substrates used in thick film techniques, e.g. platinised silicon [50] and alumina [51], can be directly used as fluid-cell carriers in USM devices because of their good biocompatibility [52–55].

In this paper, we report the development of an USM device based on screen-printed PZT 2-D 36-element (6 × 6) matrix array transducers and demonstrate the feasibility of using the thick film transducers for microparticle manipulation. All layers of the 2-D transducer array were screen-printed and sintered on an alumina substrate in the required pattern layer-by-layer. Finite element analysis (FEA) was used to predict the behaviour of the array and the multilayer resonant devices, e.g. in terms of acoustic pressure distributions. Electrical impedance spectroscopy and laser vibrometry were used to evaluate the performance of the transducer array. Particle manipulation was experimentally demonstrated with two configurations: one coupling the array to a fluid-filled bio-compatible glass capillary to test the performance of each thick film PZT element rapidly, and the other coupling the array to a fluid cavity formed between a glass reflector and the alumina substrate of the array itself, giving more dexterity to realise multi-element trapping.

2. Method

An USW can be established in a multilayer planar resonator, in which an incident ultrasound is superposed on its reflected wave [6,7]. The multilayer planar resonator reported here was formed by coupling a fluid layer and a reflector on the other side of the substrate from the thick film PZT, illustrated in Fig. 1. When an USW is present in the fluid layer (Fig. 1a), depending on the physical properties of the fluid layer and the immersed particles, and because of the acoustic radiation forces, the particles move towards either the pressure nodal or anti-nodal planes (Fig. 1b) and agglomerate above the centre of the ultrasound source in these planes. Agglomeration (Fig. 1c) occurs because of the lateral radiation forces and Bjerknes forces caused respectively by the finite width of the ultrasound source and the particle-particle interactions in the acoustic field. A thickness of one or multiple half wavelengths at the operating frequency of the thick film PZT should be selected for the fluid layer as this configuration is relatively insensitive to any change in the parameters of the other layers [6].

Acoustic radiation forces on a small, rigid and incompressible sphere subjected to an USW field in an inviscid fluid were first expressed by King [56]. Later, Yosioka and Kawasima extended King's theory to compressible spheres and expressed the time-averaged acoustic radiation force on a sphere of radius, a, as [57]:

$$F(x) = 4\pi k a^3 \left[\left(\frac{\rho_p + \frac{2}{3}(\rho_p - \rho_f)}{2\rho_p + \rho_f} \right) - \frac{\beta_p}{3\beta_f} \right] E_{ac} \sin(2kx) \quad (1)$$

where x is the distance from the particle to the pressure node; k is the wave number and is equal to $2\pi/\lambda_f$, where λ_f is the wavelength in the fluid; and ρ and β are the density and compressibility of the fluid and particle indicated by subscripts f and p respectively.

The compressibility is related to the speed of sound, c, by

$$\beta = \frac{1}{\rho c^2} \quad (2)$$

and the acoustic energy density, E_{ac}, is related to the acoustic pressure of the ultrasound standing wave, P, and is given by

$$E_{ac} = \frac{P^2}{4\rho_f c_f^2} \quad (3)$$

3. Finite element analysis

To predict the behaviour and performance of the USM device, the thick film PZT transducer array and the resonant device were modelled using a FEA package, PZFlex (Weidlinger Associates Ltd, Glasgow, UK). Both two-dimensional (2-D) and three-dimensional (3-D) models were created. The 2-D model was used to study the electrical impedance spectra of the thick film transducer and the multilayer USM device and to predict the pressure distribution through the thickness of the device. The 3-D model was used to inspect pressure distributions and predict particle trapping sites across the width of the device.

The 2-D model is shown in Fig. 2 with the layer thicknesses and key material properties listed in Table 1. The piezoelectric material properties of PZT (IKTS-PZ5100 [51,58], Fraunhofer IKTS, Germany) are listed in Table 2, with a mechanical Q-factor of 76 at 1 MHz, and the other materials were assigned properties defined in the PZFlex material libraries. The FEA mesh size was 2.75 μm, approximately 1.38% of the wavelength in water, λ_w, at the 7.5 MHz frequency of interest, and the complete model was assigned a width four times the mesh size in the x-axis and with symmetry

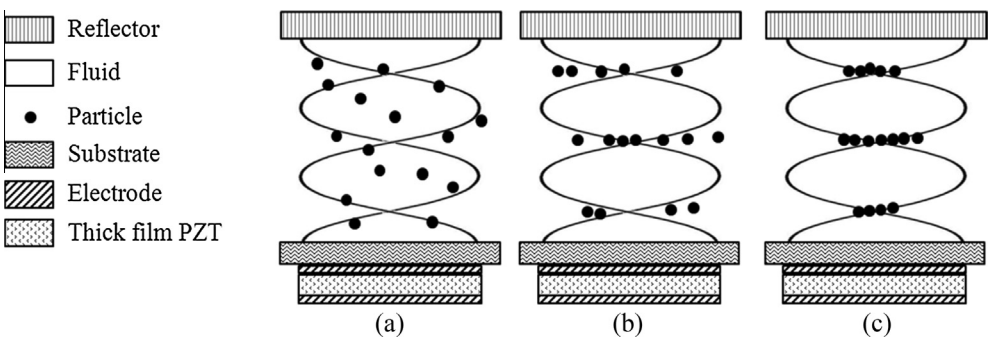

Fig. 1. Schematic diagram of configuration and operation of thick film PZT multilayer planar resonator.

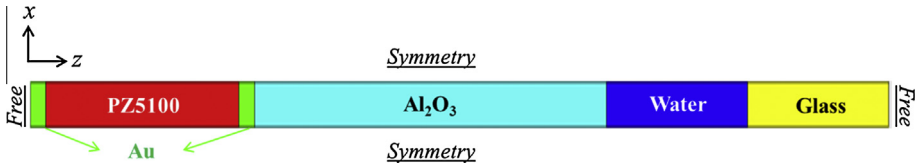

Fig. 2. 2-D PZFlex model of one element of the 2-D matrix array manipulator.

Table 1
Layer parameters in the 2-D model.

Layer	Bottom/top electrode	Thick film PZT	Substrate	Fluid layer	Reflector
Material	Gold	IKTS-PZ5100	Alumina	Water	Crown glass
Thickness (μm)	11	139	250	$n\lambda_w/2$ (n = 1, 2, 3, …)	100
Density (kg m^{-3})	19,302	6000	3920	1000	2240
Speed of sound (m s^{-1})	3240	4865	10,381	1496	5100

Table 2
Piezoelectric properties of PZT (IKTS-PZ5100): elastic stiffness constant, c_{ij}^E (10^{10} N/m^2), piezoelectric constant, e_{ij} (C/m^2) and relative permittivity, ε_{ij}^S (ε_0).

c_{11}^E	c_{12}^E	c_{13}^E	c_{33}^E	c_{44}^E	c_{66}^E	e_{15}	e_{31}	e_{33}	ε_{11}^S	ε_{33}^S
12.71	7.86	7.87	11.13	2.92	2.42	11.316	−1.704	15.99	1320	1475

boundary conditions on both sides. This 2-D model could therefore be considered close to a 1-D model because of the infinite width resulting from these symmetry conditions. Free boundary conditions were assigned to represent air beyond the minimum and maximum of the model in the z-axis. Excitation was by a short pulse, comprising a half cycle sinusoid at frequency 15 MHz, and was allowed to ring down, with oscillation decaying fully within the runtime.

The electrical impedance spectra of the models were derived from the simulated voltage and current responses, building up the complete model layer-by-layer as shown in Fig. 3. When an alumina layer was added to the thick film PZT, the thickness-mode fundamental resonant frequency of the complete transducer shifted down and a second harmonic resonance appeared (Fig. 3c and d). When a water layer was added, more resonances appeared near the transducer resonant frequencies because of the periodicity caused by the water layer (Fig. 3e and f). With a thicker water layer, a greater spectral density of the system resonances appears, superimposed on the trend of the transducer resonance (Fig. 3g and h). These system resonances were thought to be closely related to the low damping of the resonant system, linked to the fact that the ultrasound wavelength in water is much smaller than the total thickness of the water layer. A similar phenomenon has also been reported in other simulated and experimental actuators that have similar layer configurations [3,59–61]. The amplitudes of these resonances, periodic in the electrical impedance spectra, were closely related to the parallelism of the resonators [61]. In the present work, the pressure through the thicknesses of all layers was also calculated at the frequency of maximum pressure response in the water layer. Two representative pressure characteristics for the device with different water thicknesses are shown in Fig. 4, indicating USWs were formed in the water layer. The maximum time-averaged acoustic radiation force can then be calculated from the maximum pressure with Eq. (1), e.g. the force on a Ø10 μm polystyrene sphere (density ρ_s = 1050 kg m^{-3} and speed of sound c_s = 2400 m/s) in a 2 mm thick water layer is about 0.56 nN with the pressure 0.67 MPa at the frequency 7.52 MHz of 1 V_{peak} excitation.

The 3-D FEA model, Fig. 5, was created with 100 μm thickness water and the thicknesses of the other layers the same as in the 2-D model. The element pitch of the array was 2.3 mm and the dimensions of each individual PZT element were 2 × 2 mm^2 with top electrode of 1.7 × 1.7 mm^2. These dimensions gave an electrical impedance magnitude of each element approximately 50 Ω at the fundamental resonant frequency, which is convenient for electrical impedance matching to driving electronics. The FEA mesh size was 5 μm (approximately λ_w/20) in the z-axis, through the thickness of the device, and 20 μm in the x- and y-axes, because of their larger dimensions. Excitation was the same as for the 2-D model and oscillation was allowed to decay completely. As for the 2-D model, the mode shape was calculated at 6.96 MHz, the frequency of maximum response and the pressure distribution was normalised to the maximum pressure amplitude in the water layer. Pressures in the anti-nodal plane (close to the water/glass interface) and nodal plane (about 60 μm away from the water/-glass interface) are shown in Fig. 6. It can be seen that the widths at −3 dB and −6 dB relative to maximum pressure amplitude in the anti-nodal plane are approximately 0.5 mm and 1 mm respectively, thus ensuring there are no overlapping pressure gradients between two adjacent elements.

4. Experimental evaluation

4.1. Array fabrication

A PZT thick film array with the same dimensions as the models was manufactured using a screen-printing process. A series of net-shape patterned thick film layers was printed and sintered on a 100 mm × 100 mm alumina substrate with 0.25 mm thickness (99.6%, Rubalit 710, CeramTec AG, Germany) in a sequence comprising bottom Au electrode, PZT thick film, top Au electrode, dielectric insulation layer and Au electrode fan-out tracks. High grade alumina was used as the substrate to prevent degradation of the piezoelectric properties of the PZT caused by interfusion and oxidation reactions between the PZT and possible silicon content in the substrate during the sintering process [51]. Screen-printing was carried out by means of a semi-automatic screen printer (EKRA M2-K, ASYS, Germany). For the bottom and top electrodes as well as fan-out tracks, an Au-based electrode paste (C5789, Heraeus, Japan) was chosen. The electrodes were printed using a 325 mesh stainless steel screen (Koenen GmbH, Germany) with 20 μm emulsion thickness. After levelling for 10 min, the printed layers were dried at 150 °C for 10 min.

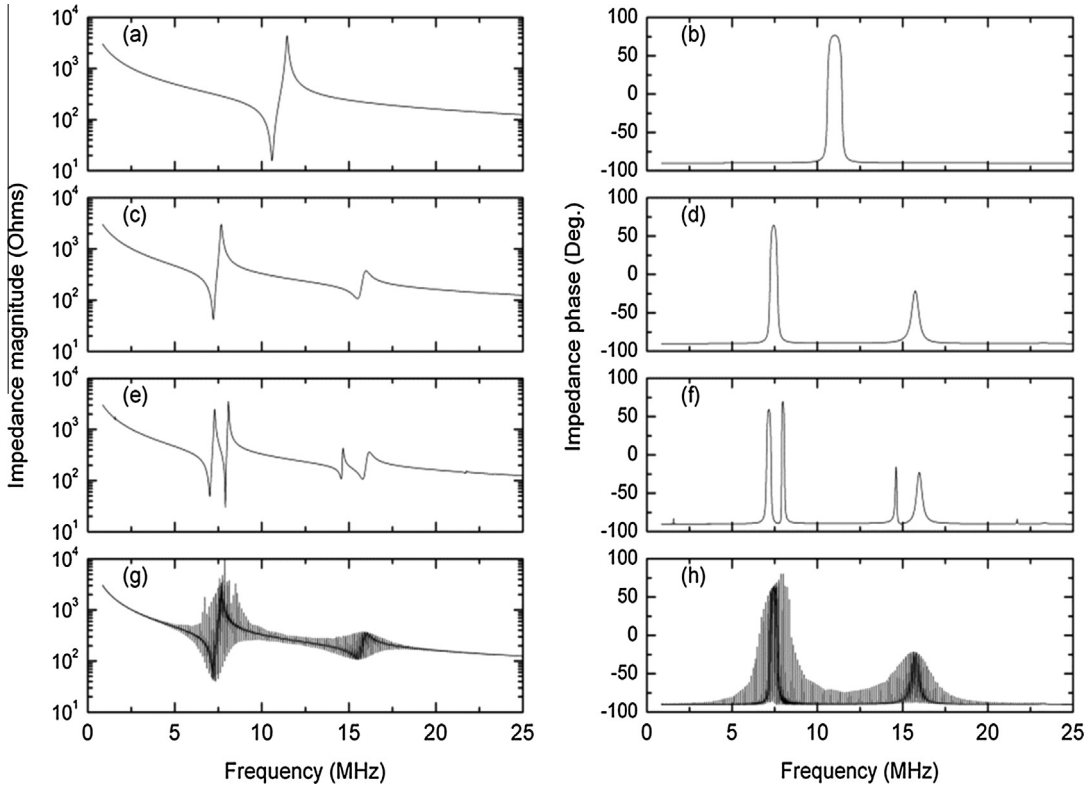

Fig. 3. Electric impedance magnitude and phase of (a, b) thick film PZ5100 layer with Au electrodes; (c, d) PZ5100 on alumina substrate; (e, f) PZ5100 with alumina, a 100-μm-thickness ($\lambda_w/2$) water layer, and a 100-μm-thickness glass reflector; and (g, h) PZ5100 with alumina, a 6000-μm-thickness ($\sim 30\lambda_w$) water layer, and a 100-μm-thickness glass reflector.

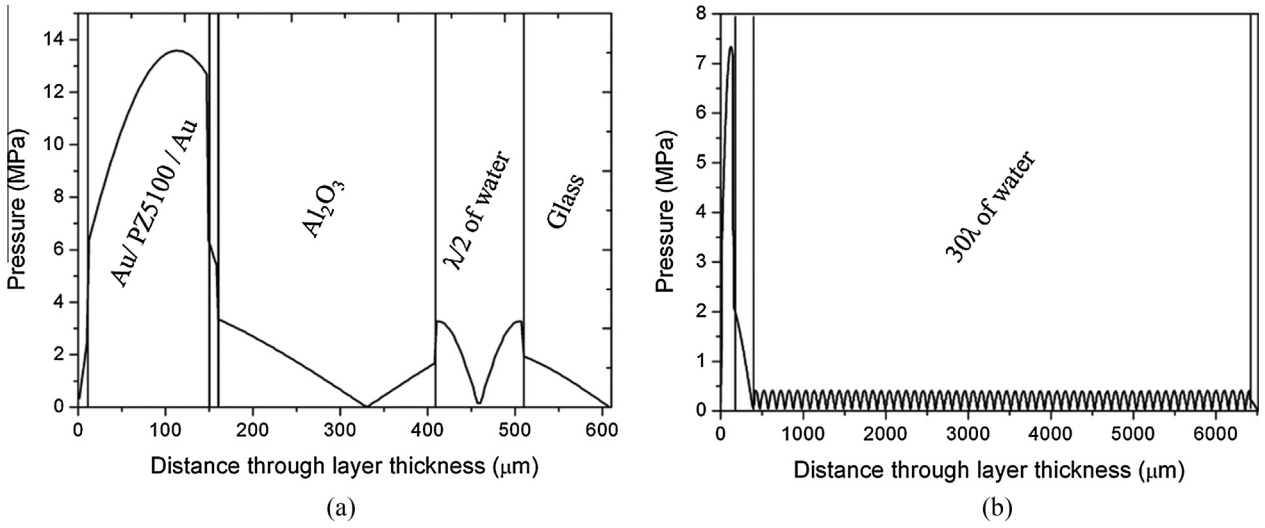

Fig. 4. Acoustic pressure through the thickness of the complete device under 1 V_{peak} excitation: device with water layer thicknesses (a) $\lambda_w/2$ and (b) $30\lambda_w$.

Sintering was carried out at 850 °C for 10 min with a total firing cycle time of 60 min. The sintered electrode thicknesses of the bottom and top electrodes as well as the fan-out tracks were measured to be approximately 11 μm.

After the bottom electrode, the piezoelectric thick film was applied. A PZT thick film paste, IKTS-PZ5100, developed at Fraunhofer IKTS was used; this is based on Sonox P51 powder (CeramTec GmbH, Germany) with the addition of a low temperature sintering eutectic mixture of Bi_2O_3 and ZnO. The content of the eutectic mixture has a significant influence on the dielectric and electromechanical properties of the PZT thick film [58]. In the present case, about 10 wt% eutectic mixture was added to the PZT powder. The PZT layer was built up by repeated screen-printing in the green state. A 200 mesh stainless steel screen (Koenen GmbH, Germany) with 20 μm emulsion thickness was applied. Five layers of PZT were printed, levelled and dried with the same conditions as mentioned above, before sintering with a heating rate of 5 K/min to 900 °C and a dwell time of two hours. The printing and sintering process was repeated to reach a final sintered thickness of 139 ± 2 μm.

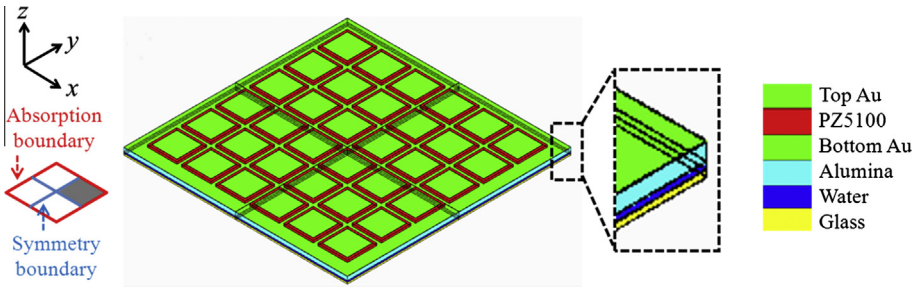

Fig. 5. A 3-D FEA model of a 2-D thick film array resonator.

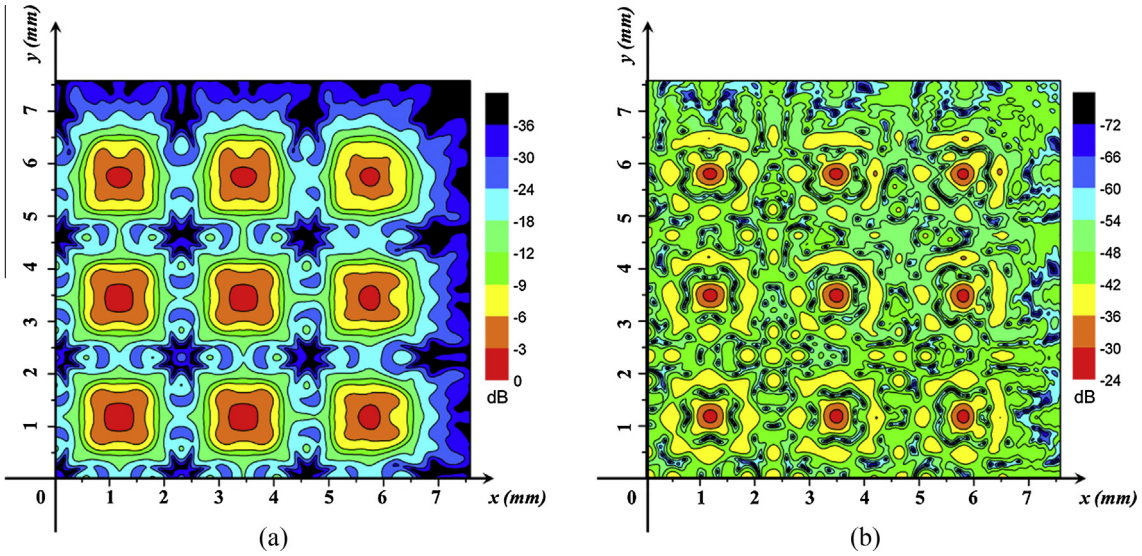

Fig. 6. Normalised pressure distributions near (a) anti-nodal and (b) nodal planes in the water layer with all elements in the device active.

Full-face top electrodes were printed and sintered on the PZT thick film as described above. The dielectric insulation layer under the electrode fan-out tracks ensured the tracks connected only to the targeted elements. Therefore, a dielectric paste (QM44D, DuPont, DE, USA) was selected. It was printed through a 200 mesh stainless steel screen (Koenen GmbH, Germany) with 20 μm emulsion thickness. The conditions for levelling, drying and sintering correspond to the process parameters used for electrode application. The process was repeated twice to ensure high insulation resistance, $>10^{11}$ Ω cm. With that, a final thickness of 40 μm was achieved.

The wafer is shown in Fig. 7 after the completion of each layer. The fabricated array was poled with a 20 kV/cm DC electric field for one minute at room temperature. The residual porosity of PZT produced with this process is usually less than 10% [58]. The measured dielectric constant and the dielectric loss were $\varepsilon_{33}{}^{T}/\varepsilon_0 = 2250 \pm 100$ and $\tan\delta = 0.09 \pm 0.005$ at 10 kHz, respectively.

4.2. Impedance spectroscopy

The electrical impedance spectrum of each element of the array was measured in air using an electrical impedance analyser (4395A, Agilent Technologies, CA, USA), as shown in Fig. 8. Similarly to the FEA results, two main resonances appeared, at frequencies of 7.4 MHz and 15.4 MHz: the lower frequency is the thickness-mode fundamental resonant frequency of the whole stack, including PZT film, electrodes, insulation layer and substrate; and the higher frequency is the 2nd harmonic of the thickness-mode of the stack. The impedance spectra indicate that screen-printing has achieved good element uniformity, although with small variations introduced by the different configurations of the dielectric insulation layer and electrode interconnection layer on the elements at different positions within the array, as shown in Fig. 9a–g. Because other layers must be added to the array to form a multilayer resonant structure and the system resonance is primarily determined by the water layer, these small variations have a negligible effect on device operation.

4.3. Laser vibrometry

The vibration behaviour and surface displacement of the array were characterised using a scanning laser vibrometer (PSV 400, Polytec GmbH, Waldbronn, Germany). A frequency range 4–20 MHz was swept to gain the amplitude response of vibration on top of the PZT. The maximum amplitude peak appeared at a frequency of 7.425 MHz, in good correspondence with the thickness-mode fundamental resonant frequency measured by the electrical impedance analyser. The surface displacement profiles of the array were mapped with selected elements driven with a 10 V_{peak} continuous sinusoid at 7.425 MHz, as shown in Fig. 10. The peak displacement was about 16 nm with a single element activated (Fig. 10a). This was much larger than the 6 nm recorded with four elements activated in a 2×2 configuration (Fig. 10b). The discrepancy may have two causes: the input power distributed over four elements, and the electrical impedance mismatch caused by the parallel connection dropping the load impedance of the four elements significantly below 50 Ω, as shown in Fig. 9h.

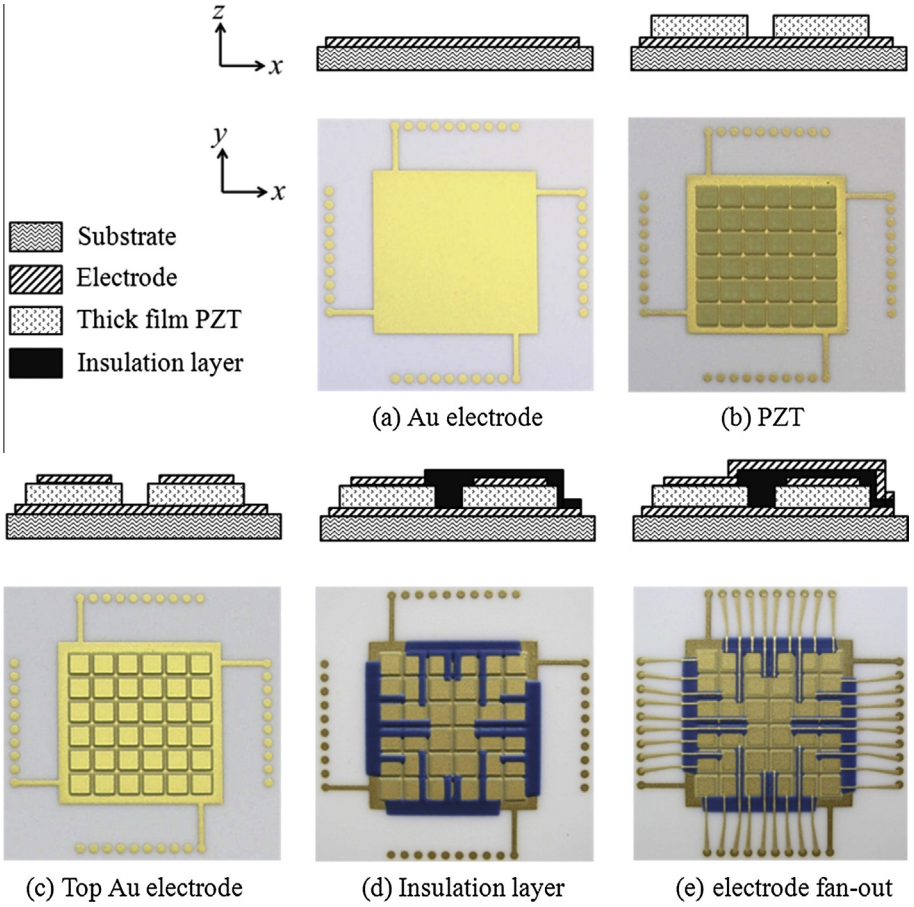

Fig. 7. Fabrication sequence for PZT thick film array: (a) completed bottom Au electrode on an alumina substrate; (b) 36 elements of thick film PZT printed on the bottom electrode; (c) top Au electrode on top of the PZT; (d) dielectric insulation layer; and (e) final electrode fan-out interconnection layer.

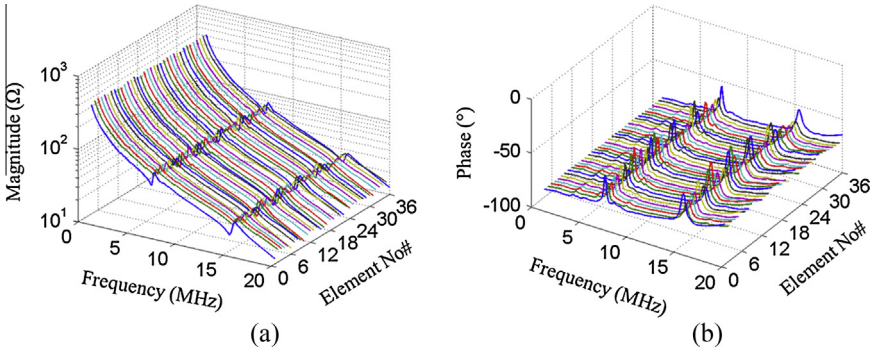

Fig. 8. Measured electrical impedance spectra of all 36 elements of the array, (a) magnitude, and (b) phase.

4.4. Particle manipulation

Simple particle manipulation experiments were carried out to evaluate the device performance. Two experimental configurations were used: one coupled the array to a fluid-filled bio-compatible glass capillary, similar to the setup described in [38], and the other coupled it to a fluid cavity chamber and a reflector to form a resonant structure, similar to the setup described in [62]. Degassed water containing Ø10 μm fluorescent polystyrene microspheres (Polysciences Inc., Warrington, PA, USA) was used in all experiments.

The feasibility of trapping with a single array element was evaluated using a glass capillary to form the resonant fluid layer. A rectangular capillary with $6.0 \times 0.3\ mm^2$ internal cross section (CM Scientific Ltd, West Yorkshire, UK) was coupled to the bare side of the alumina substrate with thin silicon grease. The electrical impedance of the whole setup was measured, giving a resonant frequency of 6.86 MHz. When an element under the capillary was driven with a signal generator (33250A, Agilent Technologies, CA, USA) producing a $10\ V_{p-p}$ continuous sinusoid at this frequency, the microspheres were instantly levitated to pressure nodal planes by the axial acoustic radiation forces and slowly agglomerated in the centre above the active element by the lateral radiation forces and Bjerknes forces, as shown in Fig. 11a. Similar results were achieved for the other elements with the same drive conditions. Furthermore, because ultrasound

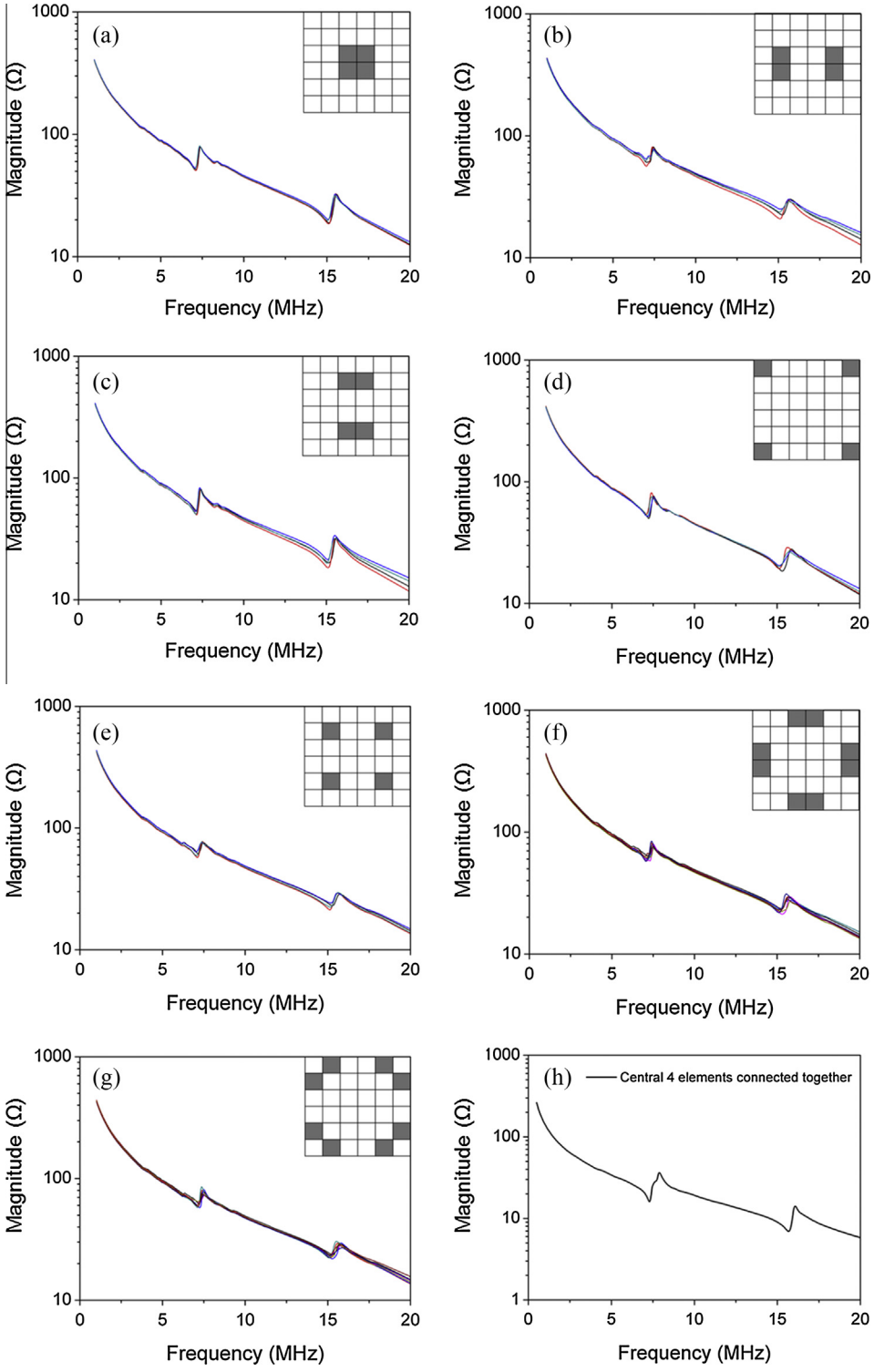

Fig. 9. Electrical impedance magnitudes of (a–g) the fabricated array elements grouped by the layer configuration and position in the array, as shown by the shaded boxes in the inset diagrams, and (h) central four elements connected together.

propagates faster in glass than in water, so the ultrasound leaking from the sidewalls of the capillary will also build up an USW between the sidewalls but with smaller pressure gradient. Therefore, the position of the trapped agglomerate can be precisely tuned between the two sidewalls of the capillary by shifting the driving frequency [63,64]. This allowed the particle agglomerate to be moved approximately ±140 μm away from the initial trapping site on the *y*-axis, as shown in Fig. 11b.

Using the chamber-reflector setup, the feasibility of trapping with multiple array elements at the same time was evaluated. The chamber was formed with a Perspex gasket of 2 mm thickness and a glass slide of 0.1 mm thickness as the reflector. The measured resonance frequency of the whole setup was 7.258 MHz. The four central elements were driven with a 7.6 V_{p-p} continuous sinusoid at the resonant frequency. When the elements were activated, four agglomerates were formed and trapped in the chamber, as shown

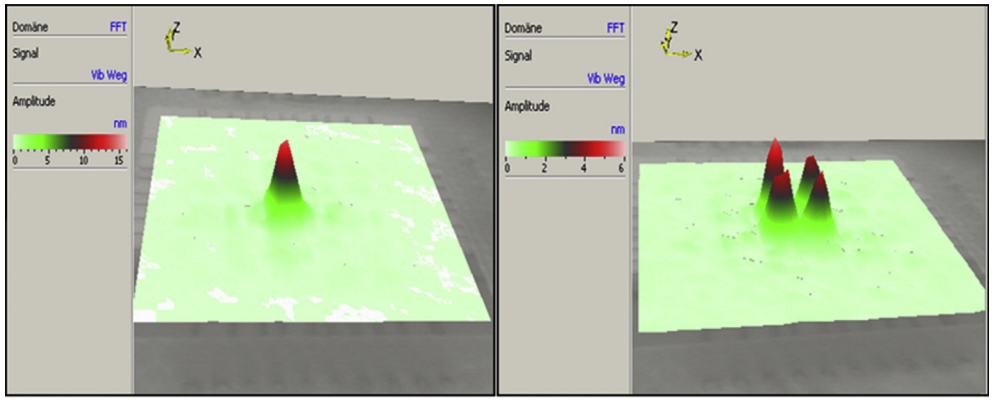

Fig. 10. Vibration profile of the thick film array with (a) one element and (b) four elements in a 2 × 2 configuration active with 10 V_{peak} continuous sinusoid at 7.425 MHz.

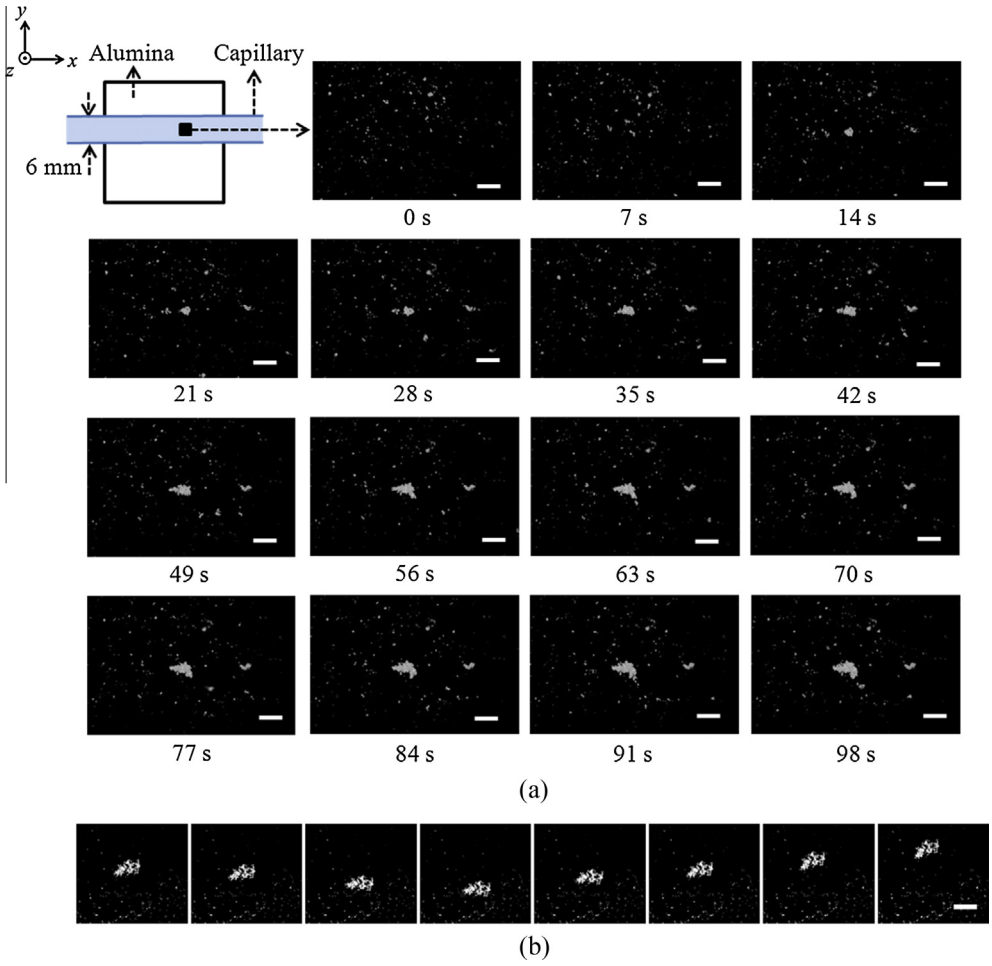

Fig. 11. Top-view image sequences of (a) microspheres being trapped and agglomerated in a pressure node in the capillary and (b) manipulation of trapped agglomerate in the *y*-axis by shifting the driving frequency. Scale bars = 200 μm.

in Fig. 12. A similar result was achieved by driving all 36 elements; however, compared to the result with four elements activated, it took much longer time to form agglomerates at the trapping sites, attributed to the weak acoustic radiation forces because of the electrical impedance mismatch caused by the parallel element connection.

5. Discussion

The electrical impedance spectra of 2-D FE models have shown the additional system resonances expected to appear when device configuration layers were added to a thick film PZT layer for multilayer USM. With a thicker water layer, a greater spectral density

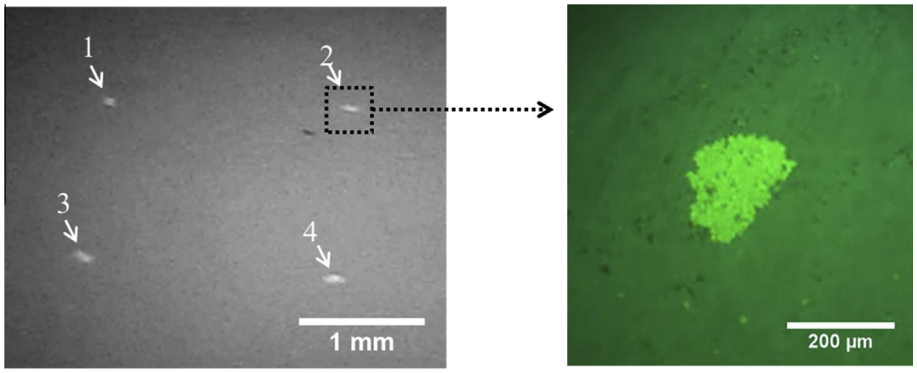

Fig. 12. Trapping with four central elements: (a) a photograph of four trapped agglomerates, and (b) a microscope image of one of the trapped agglomerates. The trapped agglomerates in Fig. 12(a) are symmetric but appear asymmetric because of the observation angle.

of the system resonances was evident, superimposed on the trend of the electrical impedance spectrum of the device itself. This was attributed to the fact that the wavelength in water at the frequency of interest is much smaller than the thickness of the water given the low damping of the complete resonant system. The pressure distributions through the thickness of the USM device indicated that USWs can be formed in the water layer. Consequently, raised acoustic radiation forces on immersed particles can move the particles to the pressure nodes or anti-nodes depending on the material properties of the particles. The maximum time-averaged acoustic radiation force on a Ø10 μm polystyrene sphere in a 2 mm thick water layer was about 0.56 nN with a pressure of 0.67 MPa at frequency 7.52 MHz for 1 V_{peak} excitation. This force was much larger than that generated by a 1-D array [38,65], where the maximum vertical force was 0.206 nN in simulation and 0.18 ± 0.06 nN in experiments with 17 $V_{p\text{-}p}$ excitation. This is because the present 2-D array generates a higher acoustic pressure and had a larger wave number, therefore leading to a much faster manipulation speed.

The 3-D FE model showed that no overlapping pressure gradients exist between two adjacent array elements, ensuring that adjacent elements cannot affect acoustic trapping performance during multiple-element trapping experiments. On the other hand, though, the lack of overlap of energy gradients indicates that the current device is unable to transport particle agglomerates laterally by switching between active array elements in the same way as other array-based USM devices [38]. However, if lateral control of particle agglomerates is essential for a proposed application, one possible solution is to reduce the element size and activate multiple elements together during operation [38].

In general, thick film PZTs are built up layer by layer in the screen-printing process to achieve a total desired thickness, resulting in tapering edges on the printed PZT. To compensate for this in the current device and to prevent possible side-effects, e.g. coupled resonant modes, the width of the top electrode of each PZT element was designed to be 0.3 mm smaller than the pillar width, giving active PZT dimensions of $1.7 \times 1.7\ mm^2$ if field fringing is ignored. These tapered edges therefore constrain the minimum element size of the 2-D matrix array. One possible solution is to introduce multiple integral electrode layers in the screen-printed PZT film, which can also improve effective piezoelectric coefficients (e.g. d_{33} [66]).

In the current device, the lateral dimensions of the array were also optimised to achieve an approximate electrical impedance of 50 Ω. This was so that simple electronics could be employed during device operation, because electrical impedance matching always plays an important role in electrical energy transmission, subsequently affecting the mechanical output of the ultrasonic devices. As shown in the results from the laser vibrometer, the maximum surface displacement with four elements activated was less than 40% of that with a single element activated. This is attributed to the input power being distributed over four elements and the electrical impedance mismatch caused by the parallel connection. External impedance matching would be possible, but this would add to the cost and complexity of any final system.

The results of the electrical impedance spectroscopy showed that excellent uniformity of thick film PZT array elements has been achieved by repeated screen-printing and sintering different materials on the substrate with different masks. In the current fabrication process, the challenges existing in electrical interconnection still limited the number of the elements of the 2-D matrix array, one promising solution is to integrate 3-D electrode fan-out structures into multiple layers of ceramic [51,67], so that the concept of printing ultrasonic transducer arrays layer by layer can be fully extended to miniaturised arrays of large numbers of elements.

Preliminary particle manipulation results with the setup based on a glass capillary has shown that such a configuration is simple to use and highly resonant. The successful trapping of particles on multiple sites with multiple array elements has also demonstrated that the screen-printed thick film PZT can generate sufficient acoustic power for USM applications.

6. Conclusions

A proof-of-concept 2-D matrix array particle manipulation device based on screen-printed thick film PZT has been developed for particle manipulation. The simplified fabrication process of 2-D matrix array and the excellent reproducibility of screen-printing technique carry the potential for bulk production of this kind of USM device, in turn opening up a broad range of applications in cell biology and analytical chemistry. Further development of the device will focus on device miniaturisation with larger numbers of elements for better control dexterity (e.g. 3-D particle transportation), implementation of complex manipulation functions (e.g. single target rotation [10]) and integration of microfluidic channels/wells into the substrate for bioanalytical applications (e.g. bioassays [68]).

Acknowledgments

This work was funded by the UK Engineering and Physical Sciences Research Council through the Electronic Sonotweezers

programme (EP/G01213X) and the German Research Foundation DFG within the Priority Program Active Micro-optics. The authors thank the Sonotweezers project partners at the Universities of Southampton, Bristol and Glasgow for their support and assistance in this research.

References

[1] A. Ashkin, J.M. Dziedzic, J.E. Bjorkholm, S. Chu, Observation of a single-beam gradient-force optical trap for dielectric particles, Opt. Lett. 11 (1986) 288–290.

[2] R. Pethig, Review article-dielectrophoresis: status of the theory, technology, and applications, Biomicrofluidics 4 (2010) 1–35, http://dx.doi.org/10.1063/1.3456626.

[3] M. Gröschl, Ultrasonic separation of suspended particles-Part I: Fundamentals, Acta Acust. United with Acust. 84 (1998) 432–447. <http://www.ingentaconnect.com/content/dav/aaua/1998/00000084/00000003/art00006> (accessed 29.08.13).

[4] M. Hill, The selection of layer thicknesses to control acoustic radiation force profiles in layered resonators, J. Acoust. Soc. Am. 114 (2003) 2654, http://dx.doi.org/10.1121/1.1616581.

[5] J. Shi, D. Ahmed, X. Mao, S.-C.S. Lin, A. Lawit, T.J. Huang, Acoustic tweezers: patterning cells and microparticles using standing surface acoustic waves (SSAW), Lab Chip. 9 (2009) 2890–2895, http://dx.doi.org/10.1039/b910595f.

[6] P. Glynne-Jones, R.J. Boltryk, M. Hill, Acoustofluidics 9: modelling and applications of planar resonant devices for acoustic particle manipulation, Lab Chip. (2012) 1417–1426, http://dx.doi.org/10.1039/c2lc21257a.

[7] Y. Qiu, H. Wang, C. Demore, D. Hughes, P. Glynne-Jones, S. Gebhardt, et al., Acoustic devices for particle and cell manipulation and sensing, Sensors 14 (2014) 14806–14838, http://dx.doi.org/10.3390/s140814806.

[8] J. Shi, X. Mao, D. Ahmed, A. Colletti, T.J. Huang, Focusing microparticles in a microfluidic channel with standing surface acoustic waves (SSAW), Lab Chip. 8 (2008) 221–223, http://dx.doi.org/10.1039/b716321e.

[9] J. Lee, S.-Y. Teh, A. Lee, H.H. Kim, C. Lee, K.K. Shung, Single beam acoustic trapping, Appl. Phys. Lett. 95 (2009) 73701, http://dx.doi.org/10.1063/1.3206910.

[10] C.E.M. Demore, Z. Yang, A. Volovick, S. Cochran, M.P. MacDonald, G.C. Spalding, Mechanical evidence of the orbital angular momentum to energy ratio of vortex beams, Phys. Rev. Lett. 108 (2012) 194301, http://dx.doi.org/10.1103/PhysRevLett. 108.194301.

[11] J. Lee, C. Lee, H.H. Kim, A. Jakob, R. Lemor, S.-Y. Teh, et al., Targeted cell immobilization by ultrasound microbeam, Biotechnol. Bioeng. 108 (2011) 1643–1650, http://dx.doi.org/10.1002/bit.23073.

[12] C.E.M. Démoré, P.M. Dahl, Z. Yang, P. Glynne-Jones, A. Melzer, S. Cochran, et al., Acoustic tractor beam, Phys. Rev. Lett. 112 (2014) 174302, http://dx.doi.org/10.1103/PhysRevLett. 112.174302.

[13] J. Hultström, O. Manneberg, K. Dopf, H.M. Hertz, H. Brismar, M. Wiklund, et al., Proliferation and viability of adherent cells manipulated by standing-wave ultrasound in a microfluidic chip, Ultrasound Med. Biol. 33 (2007) 145–151, http://dx.doi.org/10.1016/j.ultrasmedbio.2006.07.024.

[14] D. Bazou, W.T. Coakley, A.J. Hayes, S.K. Jackson, Long-term viability and proliferation of alginate-encapsulated 3-D HepG2 aggregates formed in an ultrasound trap, Toxicol. In Vitro. 22 (2008) 1321–1331, http://dx.doi.org/10.1016/j.tiv.2008.03.014.

[15] M. Wiklund, Acoustofluidics 12: biocompatibility and cell viability in microfluidic acoustic resonators, Lab Chip. 12 (2012) 2018–2028, http://dx.doi.org/10.1039/c2lc40201g.

[16] D.N. Ankrett, D. Carugo, J. Lei, P. Glynne-Jones, P.A. Townsend, X. Zhang, et al., The effect of ultrasound-related stimuli on cell viability in microfluidic channels, J. Nanobiotechnol. 11 (2013) 20, http://dx.doi.org/10.1186/1477-3155-11-20.

[17] M. Wiklund, H.M. Hertz, Ultrasonic enhancement of bead-based bioaffinity assays, Lab Chip. 6 (2006) 1279–1292, http://dx.doi.org/10.1039/b609184a.

[18] F. Petersson, L. Aberg, A.-M. Swärd-Nilsson, T. Laurell, Free flow acoustophoresis: microfluidic-based mode of particle and cell separation, Anal. Chem. 79 (2007) 5117–5123, http://dx.doi.org/10.1021/ac070444e.

[19] F. Petersson, A. Nilsson, C. Holm, H. Jonsson, T. Laurell, Separation of lipids from blood utilizing ultrasonic standing waves in microfluidic channels, Analyst 129 (2004) 938–943, http://dx.doi.org/10.1039/b409139f.

[20] N.R. Harris, M. Hill, S. Beeby, Y. Shen, N.M. White, J.J. Hawkes, et al., A silicon microfluidic ultrasonic separator, Sensors Actuat. B Chem. 95 (2003) 425–434, http://dx.doi.org/10.1016/S0925-4005(03)00448-9.

[21] A.L. Bernassau, F. Gesellchen, P.G.A. Macpherson, M. Riehle, D.R.S. Cumming, Direct patterning of mammalian cells in an ultrasonic heptagon stencil, Biomed. Microdev. 14 (2012) 559–564, http://dx.doi.org/10.1007/s10544-012-9633-z.

[22] F. Gesellchen, A.L. Bernassau, T. Déjardin, D.R.S. Cumming, M.O. Riehle, Cell patterning with a heptagon acoustic tweezer-application in neurite guidance, Lab Chip. 14 (2014) 2266–2275, http://dx.doi.org/10.1039/c4lc00436a.

[23] D. Bazou, G.A. Foster, J.R. Ralphs, W.T. Coakley, Molecular adhesion development in a neural cell monolayer forming in an ultrasound trap, Mol. Membr. Biol. 22 (2005) 229–240, http://dx.doi.org/10.1080/09687860500093396.

[24] D.C. Hocking, K.A. Garvin, D. Dalecki, Ultrasound standing wave fields for tissue engineering, J. Acoust. Soc. Am. 132 (2012) 1952, http://dx.doi.org/10.1121/1.4755185.

[25] D.A. Hughes, C.J. Weijer, Y. Qiu, C. Demore, S. Cochran, Investigating the motility of Dictyostelium discodeum using high frequency ultrasound as a method of manipulation, in: IEEE Int. Ultrason. Symp. IUS, IEEE, 2012, pp. 2002–2005. http://dx.doi.org/10.1109/ULTSYM.2012.0501.

[26] P. Mishra, M. Hill, P. Glynne-Jones, Deformation of red blood cells using acoustic radiation forces, Biomicrofluidics 8 (2014) 034109, http://dx.doi.org/10.1063/1.4882777.

[27] M. Wiklund, C. Günther, R. Lemor, M. Jäger, G. Fuhr, H.M. Hertz, Ultrasonic standing wave manipulation technology integrated into a dielectrophoretic chip, Lab Chip. 6 (2006) 1537–1544, http://dx.doi.org/10.1039/b612064b.

[28] G. Thalhammer, R. Steiger, M. Meinschad, M. Hill, S. Bernet, M. Ritsch-Marte, Combined acoustic and optical trapping, Biomed. Opt. Express. 2 (2011) 2859–2870, http://dx.doi.org/10.1364/BOE.2.002859.

[29] G. Brodie, Y. Qiu, S. Cochran, G. Spalding, M. Macdonald, Optically transparent piezoelectric transducer for ultrasonic particle manipulation, IEEE Trans. Ultrason. Ferroelectr. Freq. Control. 61 (2014) 389–391, http://dx.doi.org/10.1109/TUFFC.2014.2923.

[30] P. Glynne-Jones, M. Hill, Acoustofluidics 23: acoustic manipulation combined with other force fields, Lab Chip. 13 (2013) 1003–1010, http://dx.doi.org/10.1039/c3lc41369a.

[31] A. Neild, S. Oberti, F. Beyeler, J. Dual, B.J. Nelson, A micro-particle positioning technique combining an ultrasonic manipulator and a microgripper, J. Micromech. Microeng. 16 (2006) 1562–1570, http://dx.doi.org/10.1088/0960-1317/16/8/017.

[32] O. Manneberg, S. Melker Hagsäter, J. Svennebring, H.M. Hertz, J.P. Kutter, H. Bruus, et al., Spatial confinement of ultrasonic force fields in microfluidic channels, Ultrasonics 49 (2009) 112–119, http://dx.doi.org/10.1016/j.ultras.2008.06.012.

[33] C.R.P. Courtney, C.-K. Ong, B.W. Drinkwater, A.L. Bernassau, P.D. Wilcox, D.R.S. Cumming, Manipulation of particles in two dimensions using phase controllable ultrasonic standing waves, Proc. R. Soc. A Math. Phys. Eng. Sci. (2011), http://dx.doi.org/10.1098/rspa.2011.0269.

[34] A.L. Bernassau, C.R.P. Courtney, J. Beeley, B.W. Drinkwater, D.R.S. Cumming, Interactive manipulation of microparticles in an octagonal sonotweezer, Appl. Phys. Lett. 102 (2013) 164101, http://dx.doi.org/10.1063/1.4802754.

[35] X. Ding, S.-C.S. Lin, B. Kiraly, H. Yue, S. Li, I.-K. Chiang, et al., On-chip manipulation of single microparticles, cells, and organisms using surface acoustic waves, Proc. Natl. Acad. Sci. USA 109 (2012) 1–5, http://dx.doi.org/10.1073/pnas.1209288109.

[36] C.R.P. Courtney, B.W. Drinkwater, C.E.M. Demore, S. Cochran, A. Grinenko, P.D. Wilcox, Dexterous manipulation of microparticles using Bessel-function acoustic pressure fields, Appl. Phys. Lett. 102 (2013) 123508, http://dx.doi.org/10.1063/1.4798584.

[37] C.R.P. Courtney, C.E.M. Demore, H. Wu, A. Grinenko, P.D. Wilcox, S. Cochran, et al., Independent trapping and manipulation of microparticles using dexterous acoustic tweezers, Appl. Phys. Lett. 104 (2014) 154103, http://dx.doi.org/10.1063/1.4870489.

[38] P. Glynne-Jones, C. Demore, C. Ye, Y. Qiu, S. Cochran, M. Hill, Array-controlled ultrasonic manipulation of particles in planar acoustic resonator, IEEE Trans. Ultrason. Ferroelectr. Freq. Control. 59 (2012) 1258–1266, http://dx.doi.org/10.1109/TUFFC.2012.2316.

[39] F. Zheng, Y. Li, H.-S. Hsu, C. Liu, C. Tat Chiu, C. Lee, et al., Acoustic trapping with a high frequency linear phased array, Appl. Phys. Lett. 101 (2012) 214104, http://dx.doi.org/10.1063/1.4766912.

[40] T. Kozuka, T. Tuziuti, H. Mitome, T. Fukuda, Control of a standing wave field using a line-focused transducer for two-dimensional manipulation of particles, Japanese J. Appl. Phys., Part 1 Regul. Pap. Short Notes Rev. Pap. 37 (1998) 2974–2978, http://dx.doi.org/10.1143/JJAP.37.2974.

[41] Q. Zhou, S. Lau, D. Wu, K.K. Shung, Piezoelectric films for high frequency ultrasonic transducers in biomedical applications, Prog. Mater. Sci. 56 (2011) 139–174, http://dx.doi.org/10.1016/j.pmatsci.2010.09.001.

[42] P. Maréchal, F. Levassort, J. Holc, L.P. Tran-Huu-Hue, M. Kosec, M. Lethiecq, High-frequency transducers based on integrated piezoelectric thick films for medical imaging, IEEE Trans. Ultrason. Ferroelectr. Freq. Control. 53 (2006) 1524–1533, http://dx.doi.org/10.1109/TUFFC.2006.1665110.

[43] Y. Qiu, J. Gigliotti, M. Wallace, F. Griggio, C. Demore, S. Cochran, et al., Piezoelectric micromachined ultrasound transducer (PMUT) arrays for integrated sensing, Actuat. Imag., Sensors 15 (2015) 8020–8041, http://dx.doi.org/10.3390/s150408020.

[44] D.-W. Wu, Q. Zhou, X. Geng, C.-G. Liu, F. Djuth, K.K. Shung, Very high frequency (beyond 100 MHz) PZT kerfless linear arrays, IEEE Trans. Ultrason. Ferroelectr. Freq. Control. 56 (2009) 2304–2310, http://dx.doi.org/10.1109/TUFFC.2009.1311.

[45] B. Zhu, N.Y. Chan, J. Dai, K.K. Shung, S. Takeuchi, Q. Zhou, New fabrication of high-frequency (100-MHz) ultrasound PZT film kerfless linear array, IEEE Trans. Ultrason. Ferroelectr. Freq. Control. 60 (2013) 854–857, http://dx.doi.org/10.1109/TUFFC.2013.2635.

[46] J. Akedo, M. Lebedev, Piezoelectric properties and poling effect of Pb(Zr, Ti)O_3 thick films prepared for microactuators by aerosol deposition, Appl. Phys. Lett. 77 (2000) 1710, http://dx.doi.org/10.1063/1.1309029.

[47] D. Kuscer, F. Levassort, M. Lethiecq, A.P. Abellard, M. Kosec, Lead-zirconate-titanate thick films by electrophoretic deposition for high-frequency

ultrasound transducers, J. Am. Ceram. Soc. 95 (2012) 892–900, http://dx.doi.org/10.1111/j.1551-2916.2011.04911.x.
[48] R. Noguera, M. Lejeune, T. Chartier, 3D fine scale ceramic components formed by ink-jet prototyping process, J. Eur. Ceram. Soc. 25 (2005) 2055–2059, http://dx.doi.org/10.1016/j.jeurceramsoc.2005.03.223.
[49] M. Lethiecq, R. Lou-Moeller, J. Ketterling, F. Levassort, L.P. Tran-Huu-Hue, E. Filoux, et al., Non-planar pad-printed thick-film focused high-frequency ultrasonic transducers for imaging and therapeutic applications, IEEE Trans. Ultrason. Ferroelectr. Freq. Control. 59 (2012) 1976–1982, http://dx.doi.org/10.1109/TUFFC.2012.2416.
[50] H.D. Chen, K.R. Udayakumar, L.E. Cross, J.J. Bernstein, L.C. Niles, Dielectric, ferroelectric, and piezoelectric properties of lead zirconate titanate thick films on silicon substrates, J. Appl. Phys. 77 (1995) 3349, http://dx.doi.org/10.1063/1.358621.
[51] S. Gebhardt, D. Ernst, B. Bramlage, M. Flössel, A. Schönecker, Integrated piezoelectrics for smart microsystems – a teamwork of substrate and piezo, Adv. Sci. Technol. 77 (2012) 1–10, http://dx.doi.org/10.4028/www.scientific.net/AST.77.1.
[52] S. Kitamura, H. Ohgushi, M. Hirose, H. Funaoka, Y. Takakura, H. Ito, Osteogenic differentiation of human bone marrow-derived mesenchymal cells cultured on alumina ceramics, Artif. Organs. 28 (2004) 72–82. http://www.ncbi.nlm.nih.gov/pubmed/14720292.
[53] D.S. Finch, T. Oreskovic, K. Ramadurai, C.F. Herrmann, S.M. George, R.L. Mahajan, Biocompatibility of atomic layer-deposited alumina thin films, J. Biomed. Mater. Res. A 87 (2008) 100–106, http://dx.doi.org/10.1002/jbm.a.31732.
[54] M. Nikkhah, J.S. Strobl, E.M. Schmelz, P.C. Roberts, H. Zhou, M. Agah, MCF10A and MDA-MB-231 human breast basal epithelial cell co-culture in silicon micro-arrays, Biomaterials 32 (2011) 7625–7632, http://dx.doi.org/10.1016/j.biomaterials.2011.06.041.
[55] M.K. Bhuyan, J.I. Rodriguez-Devora, K. Fraser, T.-L.B. Tseng, Silicon substrate as a novel cell culture device for myoblast cells, J. Biomed. Sci. 21 (2014) 47, http://dx.doi.org/10.1186/1423-0127-21-47.
[56] L.V. King, On the acoustic radiation pressure on spheres, Proc. R. Soc. A Math. Phys Eng. Sci. 147 (1934) 212–240, http://dx.doi.org/10.1098/rspa.1934.0215.
[57] K. Yosioka, Y. Kawasima, Acoustic radiation pressure on a compressible sphere, Acustica 5 (1955) 167–173.
[58] D. Ernst, B. Bramlage, S. Gebhardt, A. Schönecker, O. Pabst, H.J. Schreiner, Enhanced large signal performance of PZT thick film actuators for active micro-optics, in: 2013 Jt. IEEE Int. Symp. Appl. Ferroelectr. Work. Piezoresponse Force Microsc. ISAF/PFM 2013, IEEE, 2013. pp. 5–8. http://dx.doi.org/10.1109/ISAF.2013.6748714.
[59] J. Dual, D. Möller, Acoustofluidics 4: piezoelectricity and application in the excitation of acoustic fields for ultrasonic particle manipulation, Lab Chip. 12 (2012) 506–514, http://dx.doi.org/10.1039/c1lc20913b.
[60] Y. Qiu, C. Demore, S. Sharma, S. Cochran, D.A. Hughes, K. Weijer, Multi-wavelength ultrasonic standing wave device for non-invasive cell manipulation and characterisation, in: IEEE Int. Ultrason. Symp. IUS, IEEE, 2011. pp. 188–191. http://dx.doi.org/10.1109/ULTSYM.2011.0047.
[61] D.A. Hughes, Y. Qiu, C. Démoré, C.J. Weijer, S. Cochran, Alignment of an acoustic manipulation device with cepstral analysis of electronic impedance data, Ultrasonics 56 (2015) 172–177, http://dx.doi.org/10.1016/j.ultras.2014.09.017.
[62] P. Glynne-Jones, R.J. Boltryk, N.R. Harris, A.W.J. Cranny, M. Hill, Mode-switching: a new technique for electronically varying the agglomeration position in an acoustic particle manipulator, Ultrasonics 50 (2010) 68–75, http://dx.doi.org/10.1016/j.ultras.2009.07.010.
[63] T. Kozuka, T. Tuziuti, H. Mitome, T. Fukuda, Two-dimensional acoustic micromanipulation using a line-focused transducer, in: 1997 Int. Symp. Micromechanics Hum. Sci. (Cat. No. 97TH8311), IEEE, 1997, pp. 161–168. http://dx.doi.org/10.1109/MHS.1997.768875.
[64] O. Dron, J.-L. Aider, Varying the agglomeration position of particles in a micro-channel using acoustic radiation force beyond the resonance condition, Ultrasonics 53 (2013) 1280–1287, http://dx.doi.org/10.1016/j.ultras.2013.03.012.
[65] C. Demore, Y. Qiu, S. Cochran, P. Glynne-Jones, C. Ye, M. Hill, Transducer arrays for ultrasonic particle manipulation, in: Proc. – IEEE Ultrason. Symp., IEEE, 2010, pp. 412–415. http://dx.doi.org/10.1109/ULTSYM.2010.5935702.
[66] N.R. Harris, M. Hill, R. Torah, R. Townsend, S. Beeby, N.M. White, et al., A multilayer thick-film PZT actuator for MEMs applications, Sensors Actuat. A Phys. 132 (2006) 311–316, http://dx.doi.org/10.1016/j.sna.2006.06.006.
[67] S.W. Smith, E.D. Light, Two-dimensional array transducers using thick film connection technology, IEEE Trans. Ultrason. Ferroelectr. Freq. Control. 40 (1993) 727–734, http://dx.doi.org/10.1109/58.248217.
[68] T. Lilliehorn, M. Nilsson, U. Simu, S. Johansson, M. Almqvist, J. Nilsson, et al., Dynamic arraying of microbeads for bioassays in microfluidic channels, Sensors Actuat. B Chem. 106 (2005) 851–858, http://dx.doi.org/10.1016/j.snb.2004.07.003.